*The AAPS Journal, Vol. 14, No. 3, September 2012 (© 2012)*
DOI: 10.1208/s12248-012-9348-3

*Review Article*

*Theme: ADME of Therapeutic Proteins*
*Guest Editors: Craig Svensson, Joseph Balthasar, and Frank-Peter Theil*

# Tissue Distribution Studies of Protein Therapeutics Using Molecular Probes: Molecular Imaging

**Simon-Peter Williams**[1,2]

*Received 6 February 2012; accepted 14 March 2012; published online 31 March 2012*

***Abstract.*** Molecular imaging techniques for protein therapeutics rely on reporter labels, especially radionuclides or sometimes near-infrared fluorescent moieties, which must be introduced with minimal perturbation of the protein's function *in vivo* and are detected non-invasively during whole-body imaging. PET is the most sensitive whole-body imaging technique available, making it possible to perform biodistribution studies in humans with as little as 1 mg of injected antibody carrying 1 mCi (37 MBq) of zirconium-89 radiolabel. Different labeling chemistries facilitate a variety of optical and radionuclide methods that offer complementary information from microscopy and autoradiography and offer some trade-offs in whole-body imaging between cost and logistic difficulty and image quality and sensitivity (how much protein needs to be injected). Interpretation of tissue uptake requires consideration of label that has been catabolized and possibly residualized. Image contrast depends as much on background signal as it does on tissue uptake, and so the choice of injected dose and scan timing guides the selection of a suitable label and helps to optimize image quality. Although only recently developed, zirconium-89 PET techniques allow for the most quantitative tomographic imaging at millimeter resolution in small animals and they translate very well into clinical use as exemplified by studies of radiolabeled antibodies, including trastuzumab in breast cancer patients, in The Netherlands.

**KEY WORDS:** immunoPET; molecular imaging; positron emission tomography; zirconium-89.

## INTRODUCTION

Tissue distribution studies of protein therapeutics, often monoclonal antibodies, typically require invasive sampling and quantitative recovery of the target protein from the tissue milieu. In this setting, molecular imaging offers the very attractive prospect of tracking the protein distribution through time and throughout the whole body, non-invasively, at least at the level of individual organs.

Molecular imaging might be defined as the generation of images in which the intensity at a particular point is proportional to the quantity of a specific predetermined molecular species. This is in contrast to other imaging approaches where image contrast is generated by mechanisms that have an unspecified molecular origin, such as X-ray attenuation or optical phase contrast.

Few therapeutic proteins possess intrinsic properties that permit direct molecular imaging inside the body, some theranostic (1) exceptions aside. Generally, we are forced to rely on indirect detection through molecular labels or probes coupled to the protein of interest. It is this necessary labeling step that sets up many of the strengths, limitations, and nuances of each experiment and which must be considered critically in the design of an effective study. However, these labeling techniques are easily generalized to most proteins of interest and can be used in studies from mouse to man.

Optical imaging is perhaps the most active area of label development, particularly with near-infrared fluorescent (NIRF) labels that can be detected at greater tissue depths than the visibly colored reagents employed in studies of cells and tissue slices (2). NIRF labels make whole-body studies feasible in small animals (3) and may be suitable for applications such as illuminating positive margins in real time during tumor resection surgeries (4,5). They should also allow microscopic examination of antibody distribution and the cellular origins of the signal (tumor cell *versus* macrophage, for example). However, despite the great appeal of stable labels, simplified logistics, and freedom from ionizing radiation, the inherent limitations of detection depth and difficulties with dynamic range and quantitation remain serious drawbacks to optical tomography. Ultrasound detection of optically stimulated probes (photoacoustic imaging) offers to push practical detection depths from millimeters to centimeters (6).

[1] Department of Biomedical Imaging, Genentech, Inc., 1 DNA Way, South San Francisco, California 94080, USA.
[2] To whom correspondence should be addressed. (e-mail: williams.simon@gene.com)

 

For situations where quantitative whole-body tomographic data are required, we are principally concerned with radioactive labels imaged with SPECT or (especially) PET. Perhaps deceptively familiar, these molecular imaging techniques perform much better than they did 20 or even 10 years ago, as new reagents, instruments, and image reconstruction methods have become available (7).

Figure 1 schematically illustrates an antibody labeled with lysine-linked moieties that facilitate detection by PET (Zr-89 chelated in desferrioxamine) and near-infrared fluorescence (IRDye800CW). This reagent was used in elegant dual-modality studies of antibody imaging reagents by Cohen *et al*. (4).

Various factors must be considered in the experimental design: the spatial resolution and anatomical extent required in the final images, the lifetime of a label and the duration of the study, the detection sensitivity and specificity, the relative contributions of blood and tissue, label residualization, and so on. A common starting point is matching protein and label half-lives to ensure that a radioactive label has a half-life that is long enough to provide information on the biologically relevant timescale, but not much longer, so that the radiation exposure is minimized. The relevant timescale is dictated not just by the labeled protein's behavior in a binding tissue, for example, in tumor, but also by the excess of label in the background, usually the blood pool. Having low background signal at the desired imaging time point is essential if true tissue uptake is to be conspicuous. Next, we must consider the related matter of how much protein will be injected for the experiment and if that much material can be detected in tissues given the expected distribution and clearance patterns. This is an area where high sensitivity imaging, with PET for example, buys the advantage of being able to explore trace as well as higher (therapeutic) protein dosing levels, 1 mg of antibody per patient *versus* 5 mg/kg, for example.

Broad descriptions of molecular imaging can be found by the interested reader in the literature (8,9), but this review will concentrate on a few protein labeling and molecular imaging strategies that have proven to be useful in studies of protein therapeutics and which have enduring value. In particular, the relatively recent availability of the PET isotope zirconium-89 (Zr-89) is proving to be game-changing in studies of monoclonal antibodies, in mice and men (10).

## TOPICS

### Labeling: First, Do No Harm

A label may directly perturb the function of a protein, but the reaction conditions used to introduce the label may inadvertently promote some undesirable change such as oxidation, deamidation, side-chain isomerization, or aggregation (11). The basic absence of gross changes in pharmacokinetics or molecular weight are not always sufficient characterization of labeled proteins, and binding or other functional assays may be needed to assess the integrity of an imaging probe. The case of annexin V illustrates a number of difficulties that can be encountered in trying to develop a benignly labeled protein (12) highlights the benefits that can come from site-specific labeling (13) and shows the need for binding assays that properly reflect the physiological process (14). For antibodies, ligand or cell binding assays are needed to determine the immunoreactive fraction, an important quality control parameter. The Lindmo assay (15) is very widely used for this purpose, but flattering results are easily obtained if the assay is not performed under strict conditions (16). These assays are critically dependent on knowing the true protein concentration, but the presence of a label may complicate the extinction coefficients (17) or (with chelating groups) interfere with copper-dependent Lowry and bicinchoninic acid protein assays.

Labels may also alter the protein biodistribution through non-specific changes (18) in bulk, charge, or hydrophobic interactions. This has been a major barrier to the adoption of many otherwise excellent fluorescent labels. Controlling the labeling sites and limiting the stoichiometry (19,20) should minimize the risk of immunogenicity and the problems of batch-to-batch heterogeneity, helping the validation of fluorescent labels in clinical and other critical settings (4). With optical and radioactive labels alike, incorporating more labels per protein [up to 10 of each in Sampath *et al*. (21)] gives rise to a temptingly "brighter" protein with higher specific activity

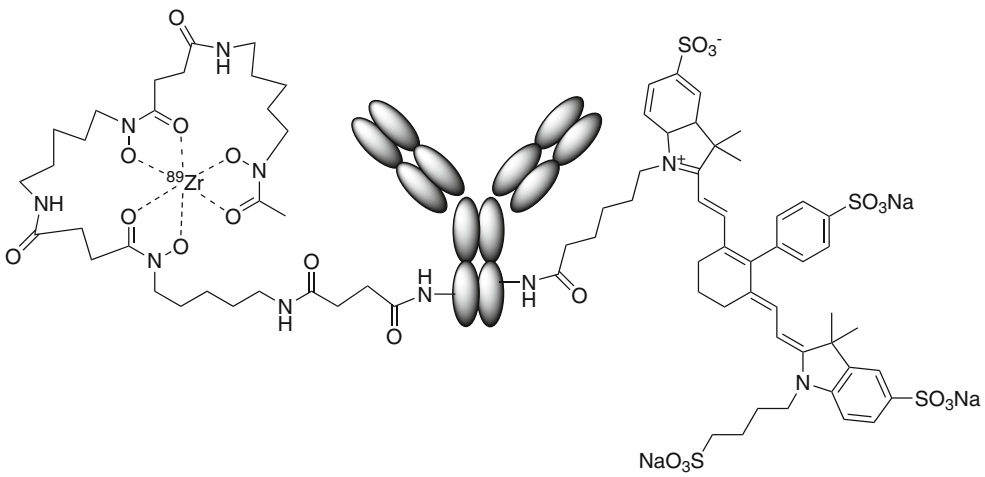


**Fig. 1.** Schematic of a dual-modality PET/optical construct used to explore the properties of IRDye800CW conjugates by Cohen at al. (4). *Left* Zr-89 chelated with desferrioxamine B. *Right* An IRDye800CW moiety. Both linked to lysine side groups on the antibody

or fluorescent yield, but this is a siren call risking compromised behavior *in vivo* (4) and would require even more cautious validation. One site-specific label per protein is the ideal.

Figure 2 illustrates a near-infrared fluorescence image in a mouse injected with a dual-modality labeled derivative of bevacizumab.

### Catabolism, Residualization, and Biological Artifacts

Any label should remain coupled to its conjugate protein for the duration of the experiment and, ideally, make no difference to its behavior, but what is the appropriate fate of a label when the protein is finally catabolized? This is a fundamental question in choosing an appropriate label for a particular experiment. The label itself will remain optically active or radioactive, and be detected in any images, but it no longer reveals the presence of the therapeutic protein *per se*. The distribution of excreted or catabolized labels can confound the imaging of certain tissues, especially in and around the hepatobiliary system and gut, the kidneys, and urinary bladder. When imaging abdominal sites, for example, this can be a limitation and has been a major driver in the selection among imaging agents based on annexin V (22,23).

Some labels are membrane permeant or are actively excreted from the catabolic cell, while others remain trapped inside the cell because of their charge and can persist for the lifetime of the cell. The iodinated labels typically fall into the first group, with iodotyrosine leaving the cell for recycling and dehalogenase enzymes scavenging the iodine for processing in the thyroid gland. These enzymes are particularly active toward iodine atoms sitting ortho- (adjacent) to a hydroxyl group on a phenyl ring, which are the product of most common iodine labeling chemistries for proteins including the indirect Bolton–Hunter reagent. Some chemical strategies have been devised to incorporate iodine labels into moieties (24–26) that resist dehalogentaion, but the protein catabolites still leave the cell. Images from proteins labeled with iodine typically include conspicuous thyroid glands due to catabolized iodine; the skin is also sometimes pronounced because of the highly active sodium/iodide symporters in that tissue. Since the iodine catabolites leave the cell, the imaging signal in the tissue reflects mostly intact protein and partial degradation products.

This property of residualizing in the cell after catabolism is possessed by most radiometal labels, which are usually lysine- or cysteine-linked to the protein of interest through chelating groups such as diethylenetriaminepentaacetic acid (DTPA), 1,4,7,10-tetraazacyclododecane-1,4,7,10-tetraacetic acid, or desferrioxamine B (DFO) (27). Upon catabolism, they tend to remain cell-trapped as charged lysine adducts (28,29). Their signal remains visible along with that of intact or partially degraded protein. Thus, the imaging signal of a residualizing label represents the current or final location of the protein, approximating the total amount accumulated at that site, comparable to measuring the area under the curve in time–activity curves obtained with non-residualizing labels. For some purposes, such as locating tissue sinks or estimating immunotoxin delivery by a targeting antibody (30), this residualizing behavior is beneficial.

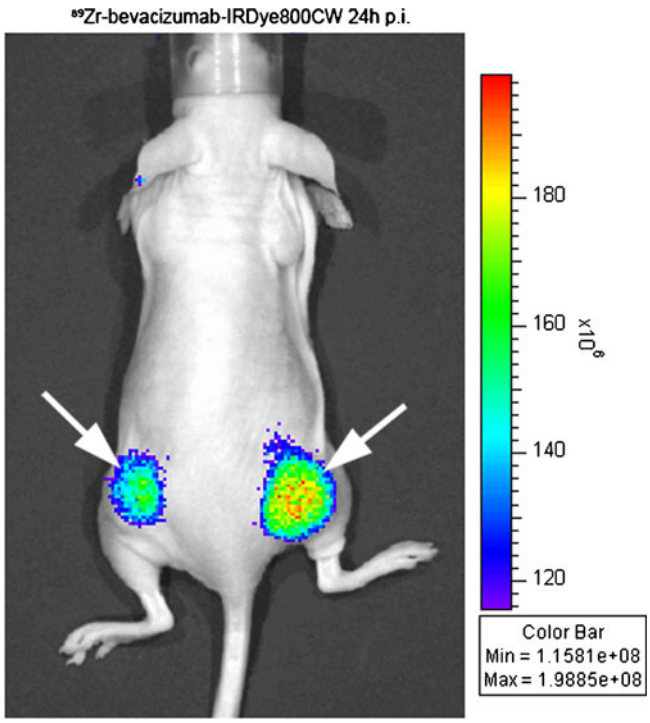


**Fig. 2.** Near-infrared fluorescence imaging with Zr89-bevacizumab-IRDye800CW from Cohen *et al.* [4]. Mouse with bilateral FaDu tumors (*white arrows*) imaged 24 h after injection with 40 μg of antibody (265 pmol, approximately 1.3 mg/kg) labeled 1:1 with IRDye800CW and 100 μCi of Zr-89. From the Zr-89 signal, it can be estimated that the signal arises from 6 to 12 pmol of dye. The image was acquired in 1 s. Despite this very sensitive detection in the superficial tumor, note the absence of signal from within the body

### Know Your Tissues: The Importance of Supporting Data

Knowledge of the tissue distribution at the organ level is useful, but sometimes insufficient. Images alone do not always sufficiently distinguish between thin tissues in close proximity, such as mineral bone and bone marrow, and follow-up experiments are required. Individual blood vessels may be resolved in the brain, but this may be insufficient to determine the fate of a labeled protein: High brain signal might be the result of protein trapped inside the cells of the blood–brain barrier, or it may result (with significantly different biological function) from protein transported and delivered into the brain parenchyma (31). Distinguishing these outcomes requires supporting information from complementary techniques. Tissue harvesting and gamma counting remain staples of preclinical validation, along with quantitative whole-body autoradiography (32).

In tumors, molecular imaging with PET can quantify the gross tumor uptake of a therapeutic antibody such as cetuximab. Figure 3 illustrates a time series of PET images from tumor-bearing mice injected with Zr-89 cetuximab. These images are informative but cannot show the spatial distribution of cetuximab relative to individual tumor cells and the capillaries supplying them. However, high-resolution spatial and compartmental information about antibody and antigen can be necessary to understanding the interplay of affinity, delivery, and efficacy (33–36). In the case of anti-

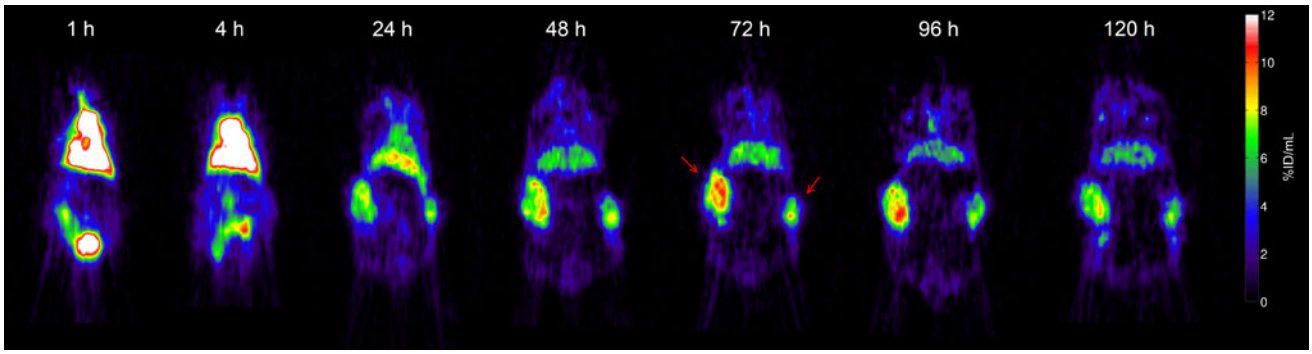


**Fig. 3.** Time series of quantitative Zr-89 cetuximab image slices in mice, from Aerts *et al.* [39]. Note the blood pool progressively clears as the bilateral HT29 tumors (*red arrows*) show progressive antibody uptake over time. The mouse was injected with 100 μg of antibody carrying 200 μCi of Zr-89 (protein dose of approximately 3.3 mg/kg), which was sufficient to obtain images out to 5 days post-injection. The scan time was 25 min. Reprinted by permission of the Society of Nuclear Medicine from Aerts *et al.* [39] (Fig. 2)

epidermal growth factor receptor antibodies, these spatial relationships (37) helped explain a puzzling lack of correlation (38–40) among expression (as immunohistochemistry), molecular imaging studies, and efficacy.

## Instrumentation and Isotopes

More detailed descriptions of radionuclide production (cyclotrons and generators), imaging instruments, and isotopes can be found in the literature cited, particularly Cherry, Sorenson, and Phelps (41); Valk, Bailey, Townsend, and Maisey (42); Sandler *et al.* (43); and von Schulthess (44). For reference, Table I presents a list of the principal radioisotopes that may be employed in the study of protein biodistribution, grouped according to the imaging modality they require and noting some pertinent properties of half-life, chemistry, and applications.

## Radiolabeling with Iodine

One of the main attractions of molecular imaging with radioiodine labels is the already widespread use of iodinated proteins, including antibodies (45,46), minimizing the need to develop and characterize novel reagents. Iodinated proteins are commonly used for measuring biodistribution through autoradiography (32,47) and in biochemical experiments such as ELISA (48) and competitive binding assays (49). Iodination chemistries can allow the preparation of labeled proteins with a very high specific activity, *i.e.*, a high level of radioactivity per mass of protein (60 mCi/mg of antibody, for example), which facilitates experiments requiring trace doses of protein. Iodine is a notably small molecular label, a single atom in its simplest form, compared to the 400 or 500 Da or more for a chelated metal or small fluorophore.

Using I-125 (60-day half-life, 35 keV energy), it is logistically easy to prepare reagents and perform experiments without tight time constraints, and the very low energy gamma rays are ideal for autoradiography in tissue slices (45). However, such low energy rays are highly attenuated by absorption and scattering in the body, making I-125 unsuitable for imaging in large animals or humans, but it can work well for small animal imaging (50) where appropriate detectors are more available.

I-123 (13-h half-life, 159 keV energy) is highly amenable to SPECT imaging (51), but its short half-life brings logistical difficulties when working with proteins and limits its application here.

I-124 (4-day half-life, 2.13 MeV positron energy; gamma rays, 0.6–1.7 MeV) offers a chemical bridge between SPECT and PET versions of the same reagent. Unfortunately, I-124 has particularly high energy positrons and extraneous gamma rays. The resultant image blurring is marked in small animals but can be improved with advanced reconstruction methods (52).

I-131 (8-day half-life; 284, 364, and 637 keV gamma rays) is a high-energy isotope that requires substantial shielding to form a properly functioning collimator. Less common in small animal scanners because of this, in humans, it has "theranostic" possibilities for simultaneous therapeutic and diagnostic imaging applications (1,53).

## Radiolabeling Proteins with Metal Ions and Fluoride Ions

Radiometal labeling is a two-step process: First, a protein is conjugated to a suitable polydentate chelating agent and stored until required; second, immediately prior to use, the radiometal is incorporated in a chelation step. This is illustrated schematically in Fig. 4. Only a small fraction, <1 %, of the chelating groups become populated with radiometal ions during the chelation step. With large proteins, unlike peptides and small molecules, there are no practical chromatographic steps to increase the specific activity by enriching the radiolabeled fraction in the final product, so optimizing the chelation reaction is the key to achieving good specific activity.

Tc-99m (half-life, 6 h; gamma energy, 140 keV) is ubiquitous in diagnostic imaging because it can be produced locally in a relatively inexpensive Mo-99 (half-life, 67 h)/Tc-99m generator. One attractive site-specific labeling strategy makes use of carbonyl chemistry and His-tags that are part of the expressed protein (54), but conventional covalently coupled chelators are available (22). The PET analog Tc-94m (half-life, 53 min; positron energy, 2.47 MeV) has poor imaging properties and is not widely used.

For antibody applications that demand a longer-lived label, there is In-111 (half-life, 3 days). This requires chelator groups (28,55) such as DTPA that are different from those

**Table I.** Major Radioisotopes of Interest for the Molecular Imaging of Protein Therapeutics

| | Half-life | Coupling chemistry | Availability | Imaged gamma ray energy (keV) | Suitable applications | Notes |
|---|---|---|---|---|---|---|
| SPECT halogens | | | | | | |
| I-123 | 13.2 h | Covalent iodination | Commercially available; iodide in NaOH | 159 | SPECT imaging of peptides, small proteins | Ideal energy for most gamma cameras; high photon yield per MBq |
| I-131 | 8.0 days | Covalent iodination | Commercially available; iodide in NaOH | 364 | Cut-and-count studies or SPECT imaging of antibodies over multiple days | Requires heavy-duty collimation and camera shielding; high radiation burden; low photon yield per MBq |
| I-125 | 60 days | Covalent iodination | Commercially available; iodide in NaOH | 35 | Cut-and-count studies, binding assays, autoradiography, small animal imaging | Readily makes high specific activity reagents |
| SPECT radiometals | | | | | | |
| Tc-99m | 6.0 h | Chelation of a complex (MAG3, HYNIC, histidine repeats) | TcO4-(pertechnetate) from Mo-99 generator; commercially available | 140 | Same-day SPECT imaging of peptides | Historically and commercially important; ubiquitous; inexpensive |
| In-111 | 67.3 h | Chelation (DTPA, DOTA) | Cyclotron; In(III) chloride commercially available | 173, 247 | SPECT imaging of antibodies over multiple days, particularly for internalizing targets where residualization is important | Go-to isotope for residualizing SPECT studies of proteins; incorporated into several diagnostic imaging antibodies |
| Ga-67 | 78.3 h | Chelation (DFO) | Cyclotron; gallium citrate widely available for lung scans | 93, 185, 300 | Not widely adopted, but possible option for SPECT imaging of antibodies over multiple days | Problematic exchange reactions with the abundant transferrin in the body |
| Lu-177 | 6.7 days | Chelation (DOTA) | Cyclotron; Lu(III) chloride commercially available | 113, 208 | RIT with theranostic (simultaneous imaging) potential | Abundant 133 keV beta particles |
| Tl-201 | 12.2 days | None available | Cyclotron; Tl(III) chloride commercially available | 80 | attractive option for dual-isotope studies but no path for protein labeling | Widely discussed as SPECT agent because of clinical ubiquity (heart scans) |
| PET halogens | | | | | | |
| F-18 | 110 min | Facile complexation with Al3+ and chelation (NOTA, NODA) | Cyclotron; sodium [F18]-fluoride widely available. | 511 | PET imaging of peptides, small proteins | Rapidly evolving technology for protein and peptide labeling applications; excellent image quality from 633 keV positron and maximum possible positron yield per MBq |
| I-124 | 4.2 days | Covalent iodination | Cyclotron; iodide in NaOH | 511 | PET imaging of antibodies over multiple days; particularly for non-internalizing targets where residualization less important | 1.5 and 2.1 MeV positron and prominent 603 keV gamma detract from image quality; low positron yield per MBq |
| PET radiometals | | | | | | |
| Ga-68 | 68 min | Chelation (DOTA, NOTA, DFO) | Ga(III) chloride typically from parent Ge-68 generator, commercially available | 511 | PET imaging of peptides | Sometimes seen as PET successor to SPECT with Tc-99m, logistic difficulties remain severe |
| Cu-64 | 12.7 h | Chelation (DTPA, DOTA, TETA) | | 511 | PET imaging of peptides, small proteins | Some 579 keV betas offer therapeutic potential; relatively low energy 653 |

**Table I.** (continued)

| | Half-life | Coupling chemistry | Availability | Imaged gamma ray energy (keV) | Suitable applications | Notes |
|---|---|---|---|---|---|---|
| | | | Cyclotron or reactor; Cu(II) chloride. Limited commercial supply | | | keV positrons give very good image quality |
| Zr-89 | 78.4 h | Chelation (DFO) | Cyclotron; Zr(IV) oxalate. Limited commercial supply | 511 | PET imaging of antibodies over multiple days; particularly for internalizing targets where residualization is important | 902 keV positrons give good image quality; 909 keV gamma rays contribute to shielding and dosimetry requirements |

These are grouped by the requisite detection technology, PET, or SPECT, and their element type, halogen, or metal, since that determines the labeling approach. Labeling chemistries are discussed further in the text. Commonly employed chelating groups are listed by their common abbreviations: *MAG3* mercaptoacetyltriglycine, *HYNIC* 6-hydrazinonicotinic acid, *DTPA* diethylenetriaminepentaacetic acid, *DOTA* 1,4,7,10-tetraazacyclododecane-*N,N′,N″,N‴*-tetraacetic acid, *NOTA* 1,4,7-triazacyclononane-*N,N′,N″*-triacetic acid, *NODA* 1,4,7-triazacyclononane-1,4-diacetate, *TETA* 1,4,8,11-tetraazacyclotetradecane- *N,N′,N″,N‴*-tetraacetic acid, *DFO* desferrioxamine B

employed with Tc-99m because of the different coordination chemistry of In-111. Several clinically approved In-111 antibody-based imaging agents exist (56–58) for scintigraphy or SPECT, and there are some suggestions that In-111 can also have dual roles in imaging (gamma ray) and therapy (Auger electron) (59).

Given the sensitivity and quantitation benefits of PET compared to SPECT systems, the use of positron-emitting rather than single photon isotopes has become more compelling, so protein labeling with PET isotopes has been an active area of recent development. Several radiometal PET isotopes have been developed and evaluated for radiolabeling peptides and proteins. As a possible alternative to Tc-99m, Ga-68 (half-life, 68 min) is a PET isotope produced in a convenient generator from Ge-68 (half-life, 9 months) that combines good imaging properties and a simple non-covalent point-of-use labeling strategy applied to peptide reagents such as somatostatin analogs (60) and Affibodies (61). Generator-produced Ga-68 was presumed to be much easier and cheaper to work with in the radiopharmacy setting than the cyclotron-produced F-18 (half-life, 110 min), which typically requires relatively complex covalent radiochemistry for labeling proteins and peptides (62–64). However, recent breakthroughs in non-covalent labeling with F-18 fluoride through chelated AlF complexes (65,66) challenge this presumption, and the longer half-life, excellent imaging properties, and wide availability of F18 fluoride could be powerful advantages.

Considerable effort has gone into making cyclotron-produced Cu-64 (half-life, 12.7 h, very similar to I-123) available in the USA (67): It has been applied to imaging the biodistribution and tissue kinetics of several antibodies in non-human primates including trace doses of anti-CEACAM-6 (68). Despite the excellent image quality at time points up to 24 h, the duration of the Cu-64 studies was limited to 3 days at most, constrained by the half-life. Its optimal application may lie with smaller antibody fragments and peptides.

## The Advent of Zirconium-89

Combining a reasonably long half-life for antibody biodistribution and tumor uptake studies with excellent PET image quality and quantitation, Zr-89 (half-life, 3.3 days) is a very significant newly available reagent for imaging tissue distribution of protein therapeutics and diagnostics (10,69). It is already proven with numerous antibodies (39,70–74) and other proteins (75,76) through the efforts of groups in The Netherlands where it has been developed in both preclinical and, with good manufacturing practices (GMP) production for tracer production and validation, in clinical settings. Although Zr-89 does have an extraneous high-energy gamma ray (909 keV), the image quality is good and the overall radiation burden is well tolerated (77). Figures 5 and 6 illustrate the use of Zr-89 trastuzumab in breast cancer patients (71), demonstrating the good signal/noise properties available 5 days after the injection of 1 mCi of tracer, and the small metastatic lesions that can be resolved. Zirconium requires new chelating agents developed (78–80) from desferrioxamine B (Df, DFO, or Desferal™), a chelator used to treat iron

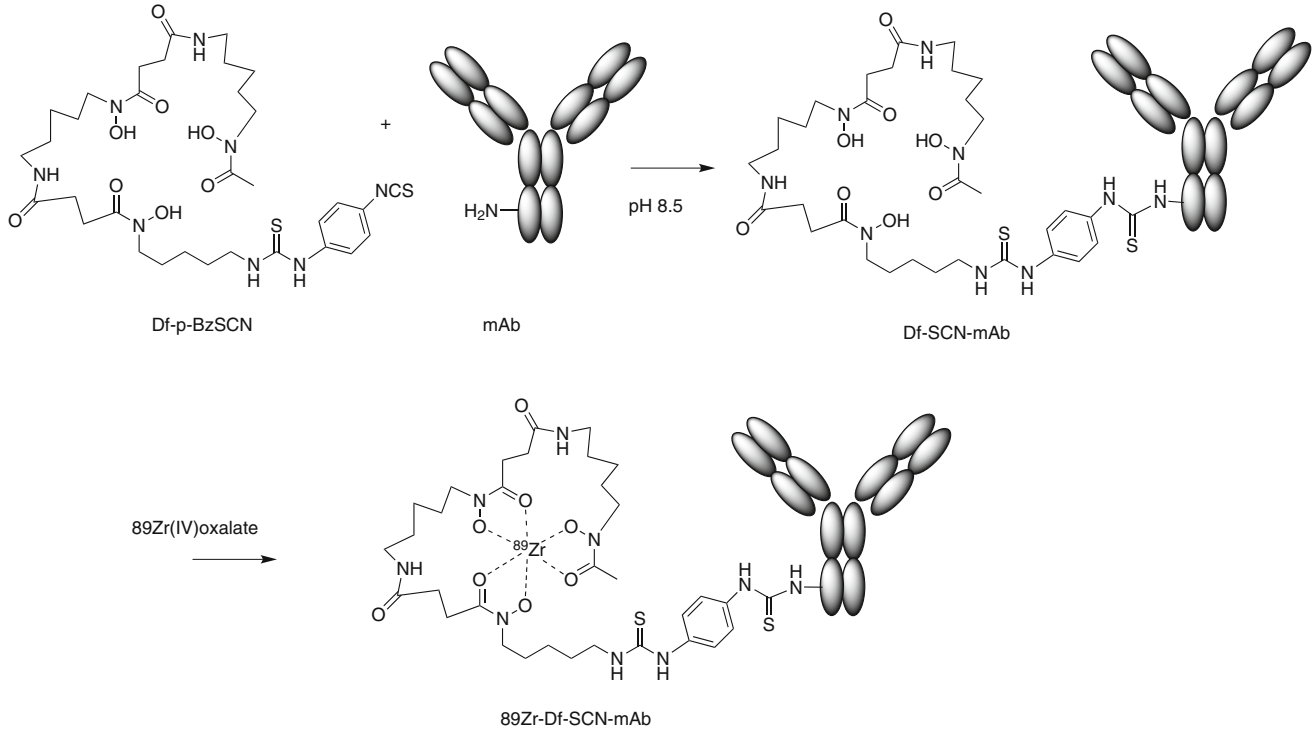


**Fig. 4.** Radiolabeling with Zr-89: covalent conjugation of a chelating group, followed later by chelation of Zr-89 at the time of use. The bifunctional (lysine-reactive, zirconium-chelating) reagent shown is the commercially available *p*-isothiocyanatobenzyl-desferrioxamine B

overload. Weakly chelated zirconium catabolites can be bone-seeking (81), leading to conspicuous signal from actively remodeling bone in mice, an artifact that can be confused with bone marrow at late time points. This does not appear to be a significant problem in patient studies.

## SINGLE-PHOTON EMISSION COMPUTED TOMOGRAPHY

Gamma ray imaging has been clinically ubiquitous for decades, first with planar scintigraphy (two-dimensional) and

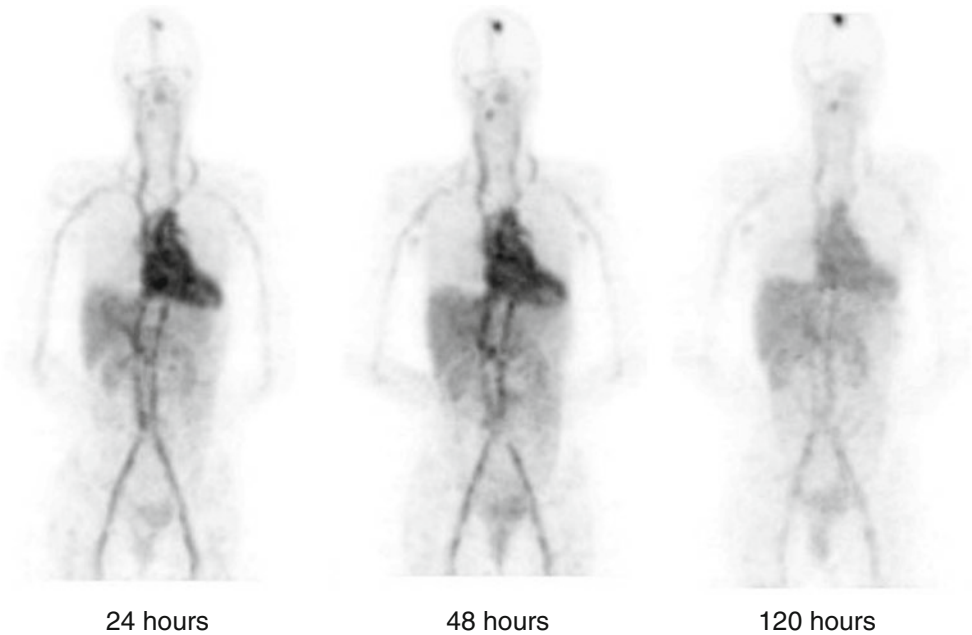


**Fig. 5.** Time series of representative Zr-89 trastuzumab images (*frontal view*) in a patient receiving trastuzumab therapy as described in Dijkers *et al.* (71). Note the heart and great vessels with blood pool diminishing slowly over 5 days. Note the absence of antibody in the brain cavity, except for blood pool and a previously undetected metastatic brain lesion that is visible at the top of the skull and shows progressive uptake over the 5 days. The injected dose was 10 mg of Zr89-trastuzumab, 38 MBq (1 mCi) of Zr-89 illustrating the sensitivity of the imaging

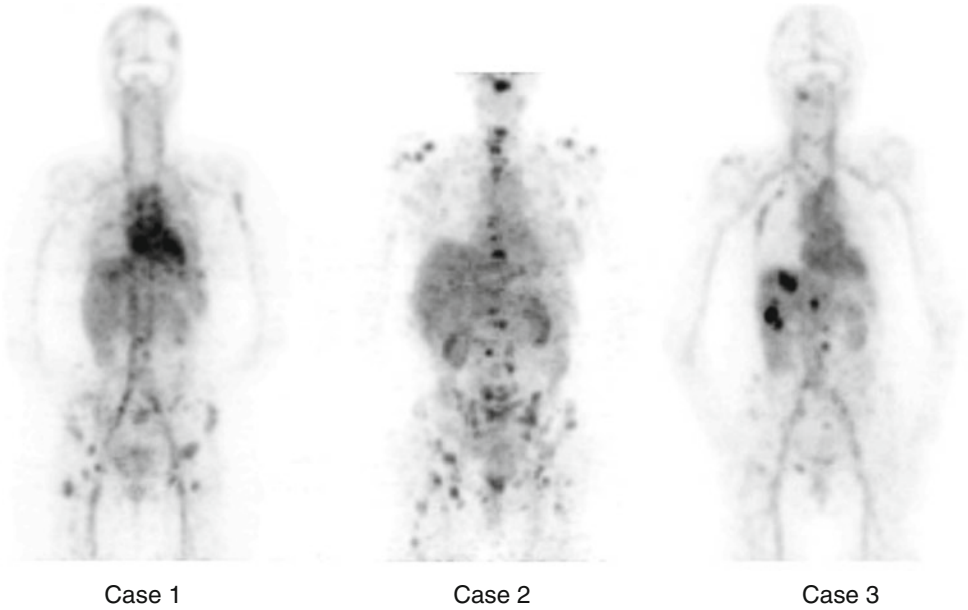


**Fig. 6.** Zr-89 trastuzumab uptake in various liver and bone lesions in three metastatic breast cancer patients as described in Dijkers *et al.* (71). The injected dose was 10 mg of Zr89-trastuzumab, 38 MBq (1 mCi) of Zr-89. Note the presence of multiple small bony and soft tissue lesions in these PET images illustrating the effective spatial resolution [from Fig. 3 in Dijkers *et al.* (71)]

more recently with SPECT (three-dimensional). One or more gamma detectors record two-dimensional projection images where the trajectory of gamma rays arriving at the detector can be deduced because they have been limited by collimation, *i.e.*, passage through narrow parallel tubes like a honeycomb or narrow apertures like a pinhole camera (82). Unfortunately, the collimation process absorbs the vast majority of the gamma rays, often more than 99 %, and the detection sensitivity is correspondingly poor compared to PET, which is performed without collimation. While sensitivity is relatively poor, image resolution can be excellent in modern SPECT instruments: Although there are trade-offs to be made in long acquisition times and high amounts of radioactivity required, resolution as fine as 0.35 mm has been demonstrated (50), better than any commercially available PET machine.

One potential benefit of SPECT is the ability to simultaneously detect and discriminate two or more isotopes by their different gamma energies (83). This is not possible with PET. However, the practical prospects of studying two or more proteins simultaneously are disappointingly limited because of the difficulties in finding two or more well-matched labels with protein-compatible half-lives, especially if residualizing labels are needed.

## POSITRON EMISSION TOMOGRAPHY

PET imaging also relies on the detection of gamma rays, but the ray trajectories are determined without collimation. Instead, PET relies on the physics of an ejected positron traveling a short distance before annihilation with an electron to yield a pair of gamma rays simultaneously flying away in opposite directions. Simultaneous events can be identified and are presumed to be the two opposing gamma rays, revealing a "line of response" between the two detector positions. A modern small animal scanner can give image resolution measured as 1.5–1.8 mm (84,85). New clinical systems can achieve spatial resolution of approximately 4 mm (86), giving richer anatomical detail in humans (diameter approximately 400 mm or 100 times the resolution) than is currently available in mice (diameter approximately 30 mm or 20 times the resolution).

Both PET and SPECT reconstruction computations can employ co-registered anatomical scans to make quantitative corrections to the image intensity and deliver images correctly calibrated in absolute units (Bq/mL). Critical to accurate quantitation in humans, this can affect even mouse scans by about 15 %.

## SUMMARY

The choice of a suitable labeling chemistry sets up the molecular imaging experiment and defines its limitations. Radionuclide imaging, particularly Zr-89 PET, offers excellent sensitivity and accurate quantitation from mouse to man, making it close to ideal for whole-body tissue distribution imaging studies for protein therapeutics with long plasma half-lives, such as monoclonal antibodies. These techniques address applications such as looking to confirm tissue delivery or to identify normal tissue sinks or rule out unexpected uptake. In small animals, there is more flexibility to use SPECT and NIRF to simplify the logistics and reduce the cost. Higher resolution complementary studies with fluorescent microscopy and autoradiography are invaluable.

## ACKNOWLEDGMENTS

I am grateful to Jan Marik for Figs. 1 and 4, Hugo Aerts for Fig. 2, Guus van Dongen for Fig. 3, and Elisabeth De Vries and Thijs Oude Munnink for Figs. 5 and 6, and for the advice of many colleagues at Genentech and elsewhere, including Jay Tibbitts, Paul Fielder, Lisa Bernstein, Ben Shen, Cinthia Pastuskovas, Leslie Khawli, Andy Boswell,

Jan Marik, Nick van Bruggen (Genentech), Simon Cherry and Julie Sutcliffe (UC Davis), Koji Iwata, and the late Bruce Hasegawa (UCSF).

**Disclosure statement** The author has no conflict of interest in this work.

## REFERENCES


1. Ambrosini V, Fani M, Fanti S, Forrer F, Maecke HR. Radiopeptide imaging and therapy in Europe. J Nucl Med. 2011;52 Suppl 2:42S–55S. Epub 2011/12/22.
2. Johnson I, Spence MTZ, editors. Molecular probes handbook—a guide to fluorescent probes and labeling technologies. 11 edn. Carlsbad: Life Technologies; 2010.
3. Vasquez KO, Casavant C, Peterson JD. Quantitative whole body biodistribution of fluorescent-labeled agents by non-invasive tomographic imaging. PLoS One. 2011;6(6):e20594. Epub 2011/07/07.
4. Cohen R, Stammes MA, de Roos IH, Stigter-van Walsum M, Visser GW, van Dongen GA. Inert coupling of IRDye800CW to monoclonal antibodies for clinical optical imaging of tumor targets. EJNMMI Res. 2011;1(1):31. Epub 2012/01/05.
5. Sevick-Muraca EM. Translation of near-infrared fluorescence imaging technologies: emerging clinical applications. Annu Rev Med. 2012;63:217–31. Epub 2011/11/01.
6. Ntziachristos V. Clinical translation of optical and optoacoustic imaging. Philos Transact A Math Phys Eng Sci. 2011;369 (1955):4666–78. Epub 2011/10/19.
7. Cherry SR. The 2006 Henry N. Wagner Lecture: of mice and men (and positrons)—advances in PET imaging technology. J Nucl Med. 2006;47(11):1735–45. Epub 2006/11/03.
8. Weissleder R, Ross BD, Rehemtulla A, Gambhir S. Molecular imaging. Shelton: People's Medical Publishing House; 2010.
9. Rudin M. Molecular imaging: principles and applications in biomedical research. London: Imperial College Press; 2005.
10. van Dongen GAMS, Vosjan MJWD. Immuno-positron emission tomography: shedding light on clinical antibody therapy. Cancer Biother Radiopharm. 2010;25(4):375–85.
11. Harris RJ, Kabakoff B, Macchi FD, Shen FJ, Kwong M, Andya JD, *et al*. Identification of multiple sources of charge heterogeneity in a recombinant antibody. J Chromatogr B Biomed Sci Appl. 2001;752(2):233–45. Epub 2001/03/29.
12. Eisenhut M, Haberkorn U. Molecular position of radiolabels and its impact on functional integrity of proteins. J Nucl Med. 2006;47 (9):1400–2.
13. Tait JF, Smith C, Levashova Z, Patel B, Blankenberg FG, Vanderheyden J-L. Improved detection of cell death *in vivo* with annexin V radiolabeled by site-specific methods. J Nucl Med. 2006;47(9):1546–53.
14. Tait J. Measurement of the affinity and cooperativity of annexin V—membrane binding under conditions of low membrane occupancy. Anal Biochem. 2004;329(1):112–9.
15. Lindmo T, Boven E, Cuttitta F, Fedorko J, Bunn Jr PA. Determination of the immunoreactive fraction of radiolabeled monoclonal antibodies by linear extrapolation to binding at infinite antigen excess. J Immunol Methods. 1984;72(1):77–89. Epub 1984/08/03.
16. Mattes MJ. Determination of antibody immunoreactive fraction. Cancer Biother Radiopharm. 2004;19(6):667–8. Epub 2005/01/25.
17. Wakankar A, Chen Y, Gokarn Y, Jacobson FS. Analytical methods for physicochemical characterization of antibody drug conjugates. MAbs. 2011;3(2):161–72. Epub 2011/03/29.
18. Boswell CA, Tesar DB, Mukhyala K, Theil FP, Fielder PJ, Khawli LA. Effects of charge on antibody tissue distribution and pharmacokinetics. Bioconjug Chem. 2010;21(12):2153–63. Epub 2010/11/09.
19. Tinianow JN, Gill HS, Ogasawara A, Flores JE, Vanderbilt AN, Luis E, *et al*. Site-specifically 89Zr-labeled monoclonal antibodies for ImmunoPET. Nucl Med Biol. 2010;37(3):289–97. Epub 2010/03/30.
20. Shen BQ, Xu K, Liu L, Raab H, Bhakta S, Kenrick M, *et al*. Conjugation site modulates the *in vivo* stability and therapeutic activity of antibody–drug conjugates. Nat Biotechnol. 2012;30:184–9
21. Sampath L, Kwon S, Ke S, Wang W, Schiff R, Mawad ME, *et al*. Dual-labeled trastuzumab-based imaging agent for the detection of human epidermal growth factor receptor 2 overexpression in breast cancer. J Nucl Med. 2007;48(9):1501–10. Epub 2007/09/06.
22. Vanderheyden JL, Liu G, He J, Patel B, Tait JF, Hnatowich DJ. Evaluation of 99mTc-MAG3-annexin V: influence of the chelate on *in vitro* and *in vivo* properties in mice. Nucl Med Biol. 2006;33 (1):135–44. Epub 2006/02/07.
23. McQuade P, Belanger MJ, Meng X, Guenther I, Krause S, Gonzalez Trotter D, *et al*. Comparison of the *in vivo* distribution of four different annexin a5 adducts in rhesus monkeys. Int J mol imaging. 2011;2011:405840. Epub 2011/06/02.
24. Khawli LA, Kassis AI. Synthesis of 125I labeled N-succinimidyl p-iodobenzoate for use in radiolabeling antibodies. Int J Radiat Appl Instrum B Nucl med biol. 1989;16(7):727–33. Epub 1989/01/01.
25. Zalutsky MR, Narula AS. A method for the radiohalogenation of proteins resulting in decreased thyroid uptake of radioiodine. Int J Radiat Appl Instrum Appl Radiat Isot. 1987;38(12):1051–5. Epub 1987/01/01.
26. Vaidyanathan G, Affleck DJ, Zalutsky MR. Radioiodination of proteins using N-succinimidyl 4-hydroxy-3-iodobenzoate. Bioconjug Chem. 1993;4(1):78–84. Epub 1993/01/01.
27. Verel I, Visser GW, Boerman OC, van Eerd JE, Finn R, Boellaard R, *et al*. Long-lived positron emitters zirconium-89 and iodine-124 for scouting of therapeutic radioimmunoconjugates with PET. Cancer Biother Radiopharm. 2003;18(4):655–61. Epub 2003/09/25.
28. Mukai T, Namba S, Arano Y, Ono M, Fujioka Y, Uehara T, *et al*. Synthesis and evaluation of a monoreactive DOTA derivative for indium-111-based residualizing label to estimate protein pharmacokinetics. J Pharm Pharmacol. 2002;54(8):1073–81. Epub 2002/08/28.
29. Perera RM, Zoncu R, Johns TG, Pypaert M, Lee FT, Mellman I, *et al*. Internalization, intracellular trafficking, and biodistribution of monoclonal antibody 806: a novel anti-epidermal growth factor receptor antibody. Neoplasia. 2007;9(12):1099–110. Epub 2007/12/18.
30. Schrama D, Reisfeld RA, Becker JC. Antibody targeted drugs as cancer therapeutics. Nat Rev Drug Discov. 2006;5(2):147–59. Epub 2006/01/21.
31. Yu YJ, Zhang Y, Kenrick M, Hoyte K, Luk W, Lu Y, *et al*. Boosting brain uptake of a therapeutic antibody by reducing its affinity for a transcytosis target. Sci Transl Med. 2011;3 (84):84ra44. Epub 2011/05/27.
32. Stout D, Pastuskovas CV. *In vitro* methods for *in vivo* quantitation of pet and SPECT imaging probes: autoradiography and gamma counting. In: Kiessling F, Pichler BJ, editors. Small Animal Imaging. Berlin Heidelberg: Springer; 2011.
33. Thurber GM, Weissleder R. Quantitating antibody uptake in vivo: conditional dependence on antigen expression levels. Mol Imaging Biol. 2011;13(4):623–32. Epub 2010/09/03.
34. Wittrup KD, Thurber GM, Schmidt MM, Rhoden JJ. Practical theoretic guidance for the design of tumor-targeting agents. Methods Enzymol. 2012;503:255–68. Epub 2012/01/11.
35. Graff CP, Wittrup KD. Theoretical analysis of antibody targeting of tumor spheroids: importance of dosage for penetration, and affinity for retention. Cancer Res. 2003;63(6):1288–96. Epub 2003/03/22.
36. Boswell CA, Ferl GZ, Mundo EE, Bumbaca D, Schweiger MG, Theil FP, *et al*. Effects of anti-VEGF on predicted antibody biodistribution: roles of vascular volume, interstitial volume, and blood flow. PLoS One. 2011;6(3):e17874. Epub 2011/03/26.
37. Niu G, Li Z, Xie J, Le Q-T, Chen X. PET of EGFR antibody distribution in head and neck squamous cell carcinoma models. J Nucl Med. 2009;50(7):1116–23.
38. Niu G, Sun X, Cao Q, Courter D, Koong A, Le Q-T, *et al*. Cetuximab-Based Immunotherapy and Radioimmunotherapy of Head and Neck Squamous Cell Carcinoma. Clin Cancer Res. 2010;16:2095–2105.
39. Aerts HJWL, Dubois L, Perk L, Vermaelen P, van Dongen GAMS, Wouters BG, *et al*. Disparity between *in vivo* EGFR

expression and 89Zr-labeled cetuximab uptake assessed with PET. J Nucl Med. 2009;50(1):123–31.
40. Chung KY, Shia J, Kemeny NE, Shah M, Schwartz GK, Tse A, *et al*. Cetuximab shows activity in colorectal cancer patients with tumors that do not express the epidermal growth factor receptor by immunohistochemistry. J Clin Oncol. 2005;23(9):1803–10. Epub 2005/01/29.
41. Cherry SR, Sorenson J, Phelps M. Physics in Nuclear Medicine. 3 ed: Saunders; 2003.
42. Valk PE, Bailey DL, Townsend DW, Maisey MN. Positron emission tomography: basic science and clinical practice. London: Springer; 2003.
43. Sandler MP, Coleman RE, Patton JA, Wackers FJT, Gottschalk A, editors. Diagnostic molecular imaging. 4th ed. Philadelphia: Lippincott Williams and Wilkins; 2003.
44. von Schulthess GK, editor. Clinical Molecular anatomic imaging. Philadelphia: Lippincott Williams and Wilkins; 2003.
45. Langenberg WG, Schlegel DE. Autoradiography with 125-I-labeled antibodies as a means of localizing TMV antigen in plant cells. Virology. 1967;32(1):167–71. Epub 1967/05/01.
46. Wilbur DS. Radiohalogenation of proteins: an overview of radionuclides, labeling methods, and reagents for conjugate labeling. Bioconjug Chem. 1992;3(6):433–70. Epub 1992/11/01.
47. Pastuskovas CV, Mallet W, Clark S, Kenrick M, Majidy M, Schweiger M, *et al*. Effect of immune complex formation on the distribution of a novel antibody to the ovarian tumor antigen CA125. Drug metabol dispos biol fate chem. 2010;38(12):2309–19. Epub 2010/09/09.
48. Ferraiolo BL, Moore JA, Crase D, Gribling P, Wilking H, Baughman RA. Pharmacokinetics and tissue distribution of recombinant human tumor necrosis factor-alpha in mice. Drug metabol dispos biol fate chem. 1988;16(2):270–5. Epub 1988/03/01.
49. Hebert CA, Luscinskas FW, Kiely JM, Luis EA, Darbonne WC, Bennett GL, *et al*. Endothelial and leukocyte forms of IL-8. Conversion by thrombin and interactions with neutrophils. J Immunol. 1990;145(9):3033–40. Epub 1990/11/01.
50. van der Have F, Vastenhouw B, Ramakers RM, Branderhorst W, Krah JO, Ji C, *et al*. U-SPECT-II: an ultra-high-resolution device for molecular small-animal imaging. J Nucl Med. 2009;50(4):599–605. Epub 2009/03/18.
51. Crunelle CL, de Wit TC, de Bruin K, Ramakers RM, van der Have F, Beekman FJ, *et al*. Varenicline increases *in vivo* striatal dopamine D(2/3) receptor binding: an ultra-high-resolution pinhole [(123)I]IBZM SPECT study in rats. Nucl Med Biol. 2012. doi:10.1016/j.nucmedbio.2011.11.006.
52. Burdette D, Albani D, Chesi E, Clinthorne NH, Cochran E, Honscheid K, *et al*. A study on PET image quality using both strong magnetic fields and a ML-EM positron range correction algorithm. IEEE Nucl Sci Conf R. 2009:3646–51.
53. Kayano D, Taki J, Fukuoka M, Wakabayashi H, Inaki A, Nakamura A, *et al*. Low-dose (123)I-metaiodobenzylguanidine diagnostic scan is inferior to (131)I-metaiodobenzylguanidine posttreatment scan in detection of malignant pheochromocytoma and paraganglioma. Nucl Med Commun. 2011;32(10):941–6. Epub 2011/08/31.
54. Waibel R, Alberto R, Willuda J, Finnern R, Schibli R, Stichelberger A, *et al*. Stable one-step technetium-99 m labeling of His-tagged recombinant proteins with a novel Tc(I)-carbonyl complex. Nat Biotechnol. 1999;17(9):897–901. Epub 1999/09/03.
55. Esteban JM, Schlom J, Gansow OA, Atcher RW, Brechbiel MW, Simpson DE, *et al*. New method for the chelation of indium-111 to monoclonal antibodies: biodistribution and imaging of athymic mice bearing human colon carcinoma xenografts. J Nucl Med. 1987;28(5):861–70. Epub 1987/05/01.
56. Petronis JD, Regan F, Lin K. Indium-111 capromab pendetide (ProstaScint) imaging to detect recurrent and metastatic prostate cancer. Clin Nucl Med. 1998;23(10):672–7. Epub 1998/10/28.
57. Bohdiewicz PJ. Indium-111 satumomab pendetide: the first FDA-approved monoclonal antibody for tumor imaging. J Nucl Med Technol. 1998;26(3):155–63. quiz 70-1. Epub 1998/10/02.
58. Conti PS, White C, Pieslor P, Molina A, Aussie J, Foster P. The role of imaging with (111)In-ibritumomab tiuxetan in the ibritumomab tiuxetan (zevalin) regimen: results from a Zevalin Imaging Registry. J Nucl Med. 2005;46(11):1812–8. Epub 2005/11/05.
59. Leyton JV, Hu M, Gao C, Turner PV, Dick JE, Minden M, *et al*. Auger electron radioimmunotherapeutic agent specific for the CD123+/CD131- phenotype of the leukemia stem cell population. J Nucl Med. 2011;52(9):1465–73. Epub 2011/08/06.
60. Prasad V, Baum RP. Biodistribution of the Ga-68 labeled somatostatin analogue DOTA-NOC in patients with neuroendocrine tumors: characterization of uptake in normal organs and tumor lesions. Q J Nucl Med Mol Imaging. 2010;54(1):61–7. Epub 2010/02/20.
61. Baum RP, Prasad V, Müller D, Schuchardt C, Orlova A, Wennborg A, *et al*. Molecular imaging of HER2-expressing malignant tumors in breast cancer patients using synthetic 111In- or 68 Ga-labeled affibody molecules. J Nucl Med. 2010;51(6):892–7.
62. Gill HS, Marik J. Preparation of 18 F-labeled peptides using the copper(I)-catalyzed azide-alkyne 1,3-dipolar cycloaddition. Nat Protoc. 2011;6(11):1718–25. Epub 2011/10/21.
63. Gill HS, Tinianow JN, Ogasawara A, Flores JE, Vanderbilt AN, Raab H, *et al*. A modular platform for the rapid site-specific radiolabeling of proteins with 18 F exemplified by quantitative positron emission tomography of human epidermal growth factor receptor 2. J Med Chem. 2009;52(19):5816–25. Epub 2009/09/10.
64. Fedorova A, Zobel K, Gill HS, Ogasawara A, Flores JE, Tinianow JN, *et al*. The development of peptide-based tools for the analysis of angiogenesis. Chem Biol. 2011;18(7):839–45. Epub 2011/08/02.
65. Liu S, Liu H, Jiang H, Xu Y, Zhang H, Cheng Z. One-step radiosynthesis of (1)F-AlF-NOTA-RGD for tumor angiogenesis PET imaging. Eur J Nucl Med Mol Imaging. 2011;38(9):1732–41. Epub 2011/05/28.
66. McBride WJ, D'Souza CA, Sharkey RM, Goldenberg DM. The radiolabeling of proteins by the [18 F]AlF method. Appl Radiat Isot. 2012;70(1):200–4.
67. McCarthy DW, Shefer RE, Klinkowstein RE, Bass LA, Margeneau WH, Cutler CS, *et al*. Efficient production of high specific activity 64Cu using a biomedical cyclotron. Nucl Med Biol. 1997;24(1):35–43. Epub 1997/01/01.
68. Strickland LA, Ross J, Williams S, Ross S, Romero M, Spencer S, *et al*. Preclinical evaluation of carcinoembryonic cell adhesion molecule (CEACAM) 6 as potential therapy target for pancreatic adenocarcinoma. J Pathol. 2009;218(3):380–90.
69. Holland JP, Sheh Y, Lewis JS. Standardized methods for the production of high specific-activity zirconium-89. Nucl Med Biol. 2009;36(7):729–39. Epub 2009/09/02.
70. Dijkers ECF, Kosterink JGW, Rademaker AP, Perk LR, van Dongen GAMS, Bart J, *et al*. Development and characterization of clinical-grade 89Zr-trastuzumab for HER2/neu immunoPET imaging. J Nucl Med. 2009;50(6):974–81.
71. Dijkers EC, Oude Munnink TH, Kosterink JG, Brouwers AH, Jager PL, de Jong JR, *et al*. Biodistribution of 89Zr-trastuzumab and PET imaging of HER2-positive lesions in patients with metastatic breast cancer. Clin Pharmacol Ther. 2010;87(5):586–92.
72. Borjesson PK, Jauw YW, Boellaard R, de Bree R, Comans EF, Roos JC, *et al*. Performance of immuno-positron emission tomography with zirconium-89-labeled chimeric monoclonal antibody U36 in the detection of lymph node metastases in head and neck cancer patients. Clinic cancer res official J Amer Assoc Cancer Res. 2006;12(7 Pt 1):2133–40. Epub 2006/04/13.
73. Gaykema SB, Brouwers AH, Hovenga S, Lub-de Hooge MN, de Vries EG, Schroder CP. Zirconium-89-trastuzumab positron emission tomography as a tool to solve a clinical dilemma in a patient with breast cancer. J Clin Oncol. 2012;30:e74–5.
74. Oude Munnink TH, Arjaans ME, Timmer-Bosscha H, Schroder CP, Hesselink JW, Vedelaar SR, *et al*. PET with the 89Zr-labeled transforming growth factor-beta antibody fresolimumab in tumor models. J Nucl Med. 2011;52(12):2001–8. Epub 2011/11/11.
75. Heuveling DA, Visser GW, Baclayon M, Roos WH, Wuite GJ, Hoekstra OS, *et al*. 89Zr-nanocolloidal albumin-based PET/CT lymphoscintigraphy for sentinel node detection in head and neck cancer: preclinical results. J Nucl Med. 2011;52(10):1580–4. Epub 2011/09/06.
76. Nagengast WB, Lub-de Hooge MN, Oosting SF, den Dunnen WF, Warnders FJ, Brouwers AH, *et al*. VEGF-PET imaging is a noninvasive biomarker showing differential changes in the tumor

during sunitinib treatment. Cancer Res. 2011;71(1):143–53. Epub 2010/11/19.
77. Borjesson PK, Jauw YW, de Bree R, Roos JC, Castelijns JA, Leemans CR, *et al*. Radiation dosimetry of 89Zr-labeled chimeric monoclonal antibody U36 as used for immuno-PET in head and neck cancer patients. J Nucl Med. 2009;50(11):1828–36. Epub 2009/10/20.
78. Verel I, Visser GW, Boellaard R, Stigter-van Walsum M, Snow GB, van Dongen GA. 89Zr immuno-PET: comprehensive procedures for the production of 89Zr-labeled monoclonal antibodies. J Nucl med official publ Soc Nucl Med. 2003;44 (8):1271–81. Epub 2003/08/07.
79. Perk LR, Vosjan MJWD, Visser GWM, Budde M, Jurek P, Kiefer GE, *et al*. p-Isothiocyanatobenzyl-desferrioxamine: a new bifunctional chelate for facile radiolabeling of monoclonal antibodies with zirconium-89 for immuno-PET imaging. Eur J Nucl Med Mol Imaging. 2009;37:250–9.
80. Meijs WE, Herscheid JD, Haisma HJ, Pinedo HM. Evaluation of desferal as a bifunctional chelating agent for labeling antibodies with Zr-89. Int J Radiat Appl Instrum Appl Radiat Isot. 1992;43 (12):1443–7. Epub 1992/12/01.
81. Abou DS, Ku T, Smith-Jones PM. *In vivo* biodistribution and accumulation of (89)Zr in mice. Nucl Med Biol. 2011;38(5):675–81. Epub 2011/07/02.
82. Beekman F, van der Have F. The pinhole: gateway to ultra-high-resolution three-dimensional radionuclide imaging. Eur J Nucl Med Mol Imaging. 2007;34(2):151–61. Epub 2006/12/05.
83. Wall JS, Richey T, Williams A, Stuckey A, Osborne D, Martin E, *et al*. Comparative analysis of peptide p5 and serum amyloid p component for imaging AA amyloid in mice using dual-isotope SPECT. Mol Imaging Biol. 2012. doi:10.1007/s11307-011-0524-0.
84. Visser EP, Disselhorst JA, Brom M, Laverman P, Gotthardt M, Oyen WJ, *et al*. Spatial resolution and sensitivity of the Inveon small-animal PET scanner. J Nucl Med. 2009;50(1):139–47. Epub 2009/01/14.
85. Bao Q, Newport D, Chen M, Stout DB, Chatziioannou AF. Performance evaluation of the inveon dedicated PET preclinical tomograph based on the NEMA NU-4 standards. J Nucl Med. 2009;50(3):401–8. Epub 2009/02/19.
86. Jakoby BW, Bercier Y, Conti M, Casey ME, Bendriem B, Townsend DW. Physical and clinical performance of the mCT time-of-flight PET/CT scanner. Phys Med Biol. 2011;56(8):2375–89. Epub 2011/03/24.